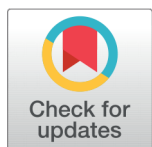


Low-temperature Electrical Properties and Correlated Barrier Hopping Conduction Mechanism in CdTiO₃



Arifa Jamil^{1,2*}, M A Rafiq¹

¹ Department of Physics and Applied Mathematics, Pakistan Institute of Engineering and Applied Sciences (PIEAS), 45650, Islamabad, Pakistan

² National Institute for Biotechnology and Genetic Engineering (NIBGE), Jhang Road, Faisalabad38000, Pakistan

 OPEN ACCESS

This article is part of the special issue on "Women in Materials Science"

Received: 14 January 2022

Accepted: 16 February 2022

Published: 30 March 2022

Editor(s): Sarish Rehman

Citation: Jamil A, Rafiq MA (2022) Low-temperature Electrical Properties and Correlated Barrier Hopping Conduction Mechanism in CdTiO₃. *Materials Innovations* 2 (3), 92-100.

* **Correspondence:** (Arifa Jamil) arifa_jamil@yahoo.com

Copyright: © 2022 Jamil A, Rafiq MA. This is an open access article distributed under the terms of the [Creative Commons Attribution License](https://creativecommons.org/licenses/by/4.0/), which permits unrestricted use, distribution, and reproduction in any medium, provided the original author and source are credited.

Published By Hexa Publishers

ISSN

Electronic: 2790-1963

CdTiO₃ nanoparticles were synthesized by solid-state reaction technique. X-ray diffraction (XRD) confirms the formation of rhombohedral CdTiO₃ nanoparticles and scanning electron microscopy (SEM) shows the irregularly shaped nanoparticles. The ac conductivity data was fitted using Jonscher's power law to find the frequency exponent "s". Correlated barrier hopping (CBH) is found to be prevailing conduction mechanism from 300 K to 160 K. The density of states (DOS) calculated by applying CBH model lie in the range of $2.89 \times 10^{20} \text{ eV}^{-1} \text{ cm}^{-3}$ to $2.96 \times 10^{21} \text{ eV}^{-1} \text{ cm}^{-3}$. The calculated minimum hopping distance (R_{min}) was $2.13 \times 10^{-9} \text{ m}$. The low values of tangent loss (< 1) at all temperatures suggest CdTiO₃ as a potential material in electrical devices with low energy losses. The shifting of maxima towards higher frequencies with the decrease in temperature in imaginary modulus plots suggests the thermally triggered hopping process in CdTiO₃ nanoparticles. The modulus studies confirm that hopping is the dominant conduction mechanism in CdTiO₃ nanoparticles as suggested by ac conductivity studies.

Keywords: Correlated barrier hopping, Density of states, Energy losses, Electrical modulus, AC conductivity

Introduction

Titanium containing oxides have aroused interest in various industrial disciplines including gas sensing, chemical and biomedical, aerospace, electronics and automotive due to their outstanding characteristics such as high specific strength, low density, good thermal stability, biocompatibility, high melting point and high resistance against corrosion.^{1,2} Low cost, chemical stability, non-toxicity and eco-friendly characteristics of titanium containing oxides

make them potential members of the research community.³ CdTiO₃ is an utmost significant member of the titanium containing oxides family having excellent dielectric, optical, electrical, ferroelectric, piezoelectric, photoresistive and sensing characteristics.⁴ The synthesis method and annealing temperature affect the crystal of CdTiO₃. The literature study showed that it crystallizes into a rhombohedral ilmenite phase (non-ferroelectric) when sintered less than 1000 °C and orthorhombic perovskite phase (ferroelectric phase) over

1000 °C. Both ilmenite and perovskite phases differ slightly in their symmetry, the structure of perovskite is asymmetric in nature having : $a = 5.348 \text{ \AA}$, $b = 7.615 \text{ \AA}$ and $c = 5.417 \text{ \AA}$, while the ilmenite structure comprises of three-fold axis with $a = b = 5.2403 \text{ \AA}$ and $c = 14.838 \text{ \AA}$.^{5,6}

The wider bandgap of CdTiO₃ makes it suitable for electric, photocatalytic, sensing, and optical applications.^{7,8} Investigation of temperature dependent electrical characteristics are fundamentals for electrical device fabrication such as energy storage devices, memory devices, spintronics and actuators. Therefore, we carried out detailed study of frequency and temperature dependent ac conductivities, CBH conduction mechanism, DOS, minimum hopping distance (R_{min}), calculations and fitting by applying CBH model on experimental data. To our knowledge, these frequency and temperature dependent parameters have not been reported for CdTiO₃ nanoparticles. Therefore, we use solid state reaction method to synthesize CdTiO₃ nanoparticles without any use of surfactant. XRD and SEM confirm the purity, crystallographic structure and physical features of CdTiO₃ nanoparticles. Low temperature (300 K-160 K) ac electrical measurements at varying frequency were performed to investigate electrical and dielectric characteristics, conduction mechanism, density of states and modulus properties in CdTiO₃ nanoparticles.

EXPERIMENTAL SETUP

Solid-state reaction technique was used to prepare CdTiO₃ nanoparticles. Titanium dioxide and cadmium acetate (purity > 99.9% acquired from Sigma-Aldrich, USA) and were used as precursor materials and mixed together in stoichiometric proportions. The mixture was grinded using agate mortar for 1 hour to get homogeneous powder. Annealing of the powder was carried

out for 3 hours at 900 °C in a box furnace in air environment. Pellets having diameter 10 mm and thickness 2 mm were formed under a load of 3 tons. Pellets were then sintered for 3 hours at 400°C for the suppression of internal stresses and eradicate crystalline defects on planes. The silver paste contacts separated by about 8mm were formed for electrical measurements. The crystalline structure and purity of synthesized CdTiO₃ were examined by Bruker D8 advance X-ray diffractometer with Cu K α radiation ($\lambda = 1.5418 \text{ \AA}$) functioned at 40 mA and 40 kV. The surface morphology was obtained by scanning electron microscope (JEOL JSM-6360) operated at an accelerating voltage 0.5-30 keV with resolution 4 nm. Agilent E4980A LCR meter was used to perform electrical measurements of CdTiO₃ nanoparticles.

RESULTS AND DISCUSSION

All the diffraction peaks in the XRD spectrum shown in Figure 1(a) were indexed to rhombohedral CdTiO₃ with no impurity peak in accordance with JCPDS card number 00-029-0277. The lattice parameters are $a = b = 5.2403 \text{ \AA}$, $c = 14.8380 \text{ \AA}$. The texture coefficient (TC) was calculated for all crystallite planes to determine the preferred orientation along the plane for CdTiO₃ nanoparticles by the relation that is often called Harris formula and modified by Mueller, Chernock and Beck and is given as⁹:

$$TC(hkl) = \frac{I(hkl)}{I_r(hkl)} \times \left(\frac{1}{n} \sum_n \frac{I(hkl)}{I_r(hkl)} \right)^{-1} \quad (1)$$

Where $I(hkl)$ is peak intensity taken from XRD spectrum of CdTiO₃, $I_r(hkl)$ denotes the reference peak intensity attained from JCPDF 00-029-0277 and n denotes the total reflection number in XRD pattern. $TC(hkl) \leq 1$ for randomly oriented planes and $TC(hkl) > 1$ for materials with preferentially oriented planes¹⁰. Table 1 shows the com-

puted $TC(hkl)$ for CdTiO₃ planes. For the (122) plane, TC value is 6.46 that is greater than 1 and maximum in the calculated values for CdTiO₃ nanoparticles and hence is preferentially oriented plane. The SEM image in Figure 1(b) shows the irregularly shaped nanoparticles having different diameters.

The frequency dependent variation of ac conductivity from 300 K to 160 K is shown in Figure 2(a) and (b). The ac conductivity of CdTiO₃ increases as temperature increases that is due to rise in drift motion of charge carriers. The rise in electrical conductivity with the increase in temperature shows thermally activated process in CdTiO₃ that specifies the semiconductor behaviour¹¹.

The increase in frequency of ac signal facilitated the transfer of charge carriers among different localized states. Moreover, trapped charges experience higher force at high frequencies and as soon the force goes above the trapped energy, confined charges are liberated resulting in increased conductivity. This leads to an increase in ac conductivity with the increase in frequency^{12,13}.

The total ac conductivity is:

$$\sigma'_{ac} = \sigma_1(T) + \sigma_2(\omega, T) \quad (2)$$

where $\sigma_1(T)$ represents temperature dependent dc conductivity and $\sigma_2(\omega, T)$ is ac conductivity that is frequency and temperature dependent and follows Jonscher's power law¹⁴:

$$\sigma_2(\omega, T) = B(T) \omega^s(T) \quad (3)$$

where B is the material's constant defining the polarizability of the material having units as that of electrical conductivity and parameter "s" is dimensionless that defines the interaction between lattice and mobile ions in the material¹⁵. The relationship between "s" and temperature can be used to investigate the material's conduction process. Several theoretical conduction models based on the behaviour of the exponents s have been presented in the literature, including

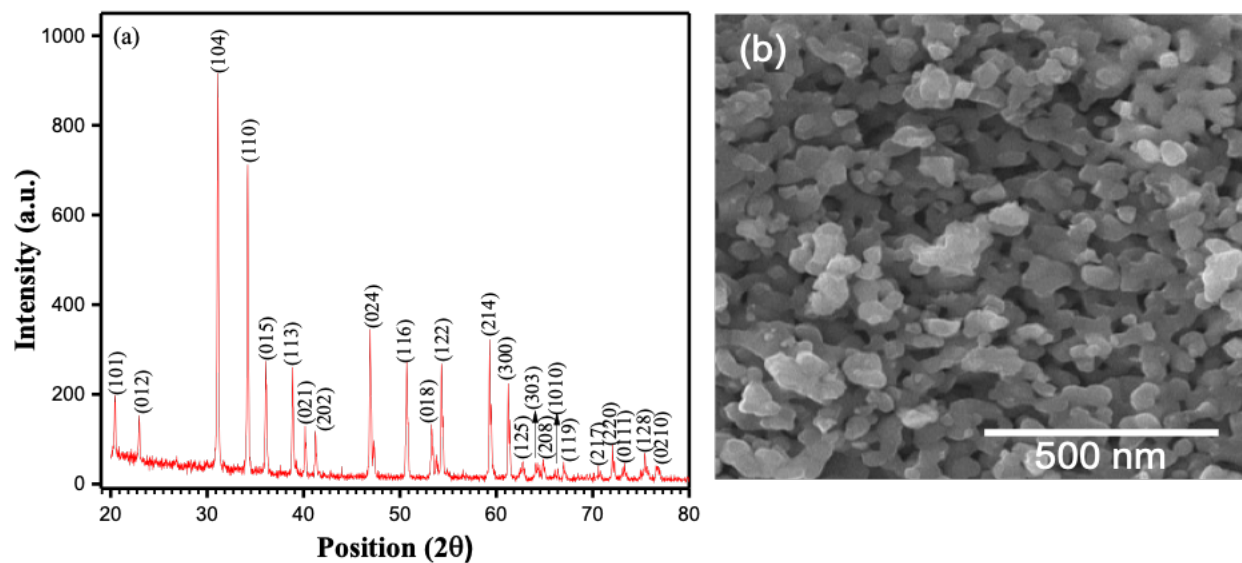


Figure 1. (a) XRD spectrum (b) SEM micrograph of CdTiO₃ nanoparticles.

Table 1. Texture coefficient for rhombohedral CdTiO₃.

h	k	l	IXRD	ICard	Texture coefficient
1	0	1	17.04	7	1.1188
0	1	2	10.57	14	0.347
1	0	4	100	100	0.4596
1	1	0	77.43	70	0.50838
0	1	5	27.34	7	1.79507
1	1	3	23.89	25	0.43919
0	2	1	12.34	10	0.56715
2	0	2	10.7	1	4.91773
0	2	4	32.64	35	0.42861
1	1	6	29.02	25	0.5335
0	1	8	11.05	14	0.36276
1	2	2	28.83	2	6.62515
2	1	4	32.5	30	0.4979
3	0	0	23.84	20	0.54784
1	2	5	4.31	3	0.66029
3	0	3	3.79	2	0.87094
2	0	8	5.16	4	0.59289
1	0	10	5.49	6	0.42053
1	1	9	3.9	4	0.44811
2	1	7	3.41	4	0.39181
2	2	0	6.28	8	0.36079
0	1	11	2.19	3	0.33551
1	2	8	6.6	6	0.50556
0	2	10	2.86	5	0.26289

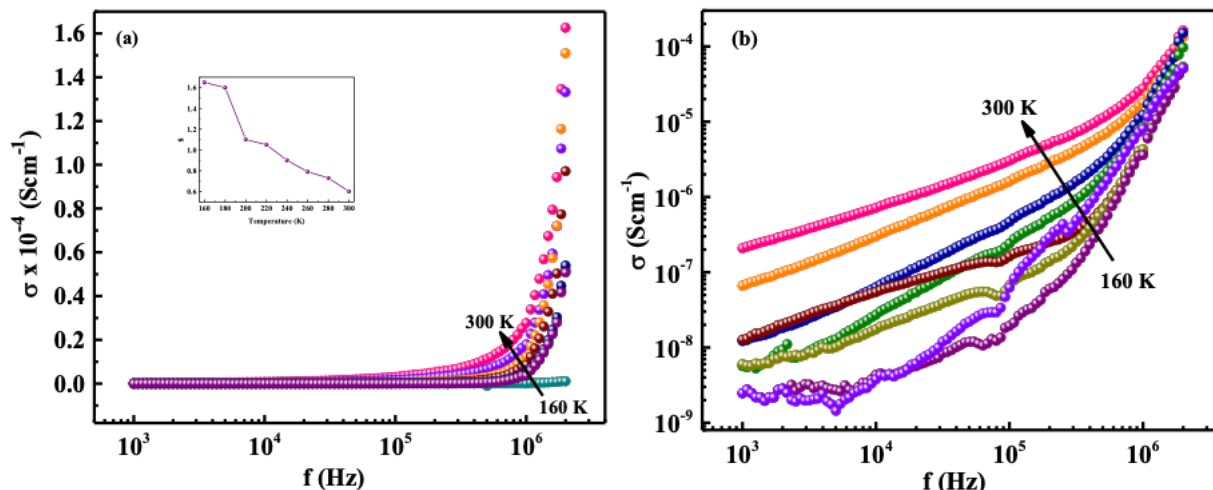


Figure 2. Frequency dependent ac conductivity (a) linear scale (b) log-log scale of CdTiO₃ nanoparticles. The inset shows temperature dependent variation of parameter "s".

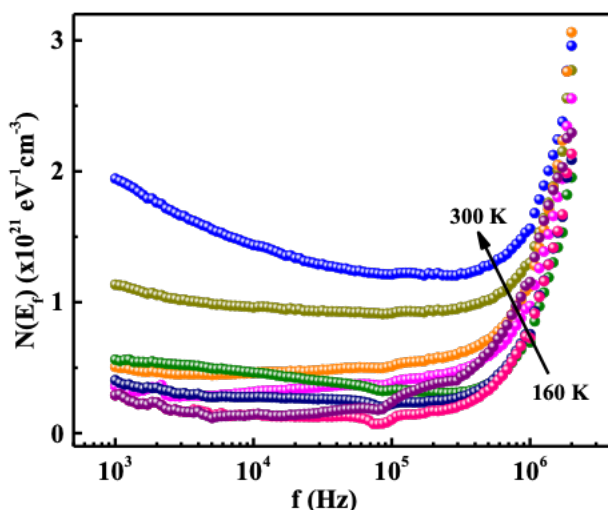


Figure 3. Variation of $N(E_f)$ with frequency for CdTiO₃ nanoparticles.

correlated barrier hopping¹⁶, overlapping large polaron tunneling¹⁷, small polaron conduction¹⁸, and quantum mechanical tunneling model¹⁹. The frequency dependent region immediately after frequency independent region in Figure 2(a) was fitted with equation 3 to obtain the power exponent "s" and shown to inset Figure 2 (a). We have to find the appropriate conduction model for CdTiO₃ based on the temperature dependence of parameter s. Accordingly, small polaron conduction model is suggested when s rises

with the rise in temperature, conduction mechanism will be OLPT in the material when increasing temperature causes decrease in "s", getting a minimum value after that it increase with the increase in temperature. If there is no change in the value of "s" with the temperature then quantum mechanical tunneling will be the conduction mechanism in the material²⁰. As these are not the case for the present study of CdTiO₃ nanoparticles so these models are not valid conduction mechanisms for CdTiO₃. Concerning the

correlated barrier hopping model, the rise in temperature results a reduction in "s" values that is the case in the present study for CdTiO₃ nanoparticles. Therefore, conduction mechanism in CdTiO₃ nanoparticles is CBH. The CBH model suggests that electron transfer is a thermally triggered process that involves hopping between two sites. As a result, short-range translational type hopping of charge carriers causes electrical conduction in the system²¹. The binding energy W_m for CBH mechanism is calculated by²²:

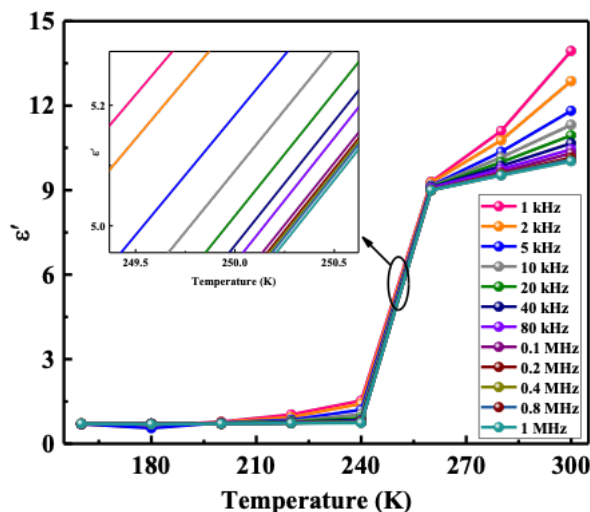


Figure 4. Temperature dependent variation of ϵ' at different frequencies for CdTiO₃ nanoparticles.

$$s = 1 - \beta \tag{4}$$

where

$$\beta = 6k_B T / W_m \tag{5}$$

The binding energy values obtained from equation (5) are used to calculate R_{min} ²²:

$$R_{min} = 2e^2 / \pi \epsilon_0 \epsilon W_m \tag{6}$$

where ϵ represents dielectric constant of CdTiO₃ and ϵ_0 stands for free space permittivity. The R_{min} values are in the range of 2.13×10^{-9} m - 1.29×10^{-7} m.

The density of states at the Fermi level $N(E_f)$ have calculated (300 K to 160 K) using ac conductivity values for CdTiO₃ by using the relation²³:

$$\sigma_{ac}(\omega) = \frac{\pi}{3} e^2 \omega k_B T (N(E_f))^2 \times \alpha^{-5} \left(\ln \left(\frac{f_0}{\omega} \right) \right)^4 \tag{7}$$

where α is localized wave function ($\alpha = 10^{10} \text{ m}^{-1}$) and f_0 is photon frequency ($f_0 = 10^{13} \text{ Hz}$)^{22,24}.

The frequency dependence of $N(E_f)$ is shown in Figure 3 from 300 K to 160 K. The DOS values decreases as frequency increases, then it begins

to increase as frequency increases, so, we get minima that moves towards lower frequency side with the decrease in temperature. The DOS decreases as frequency increases because charge carriers get sufficient energy to liberate from different trapping centers with the increase in frequency but they contain insufficient energy to cross grain boundaries and hence accumulate at grain boundaries. Further increase in frequency provide enough energy to charge carriers to cross the grain boundaries that results in the increase in DOS. A similar variation of $N(E_f)$ with frequency was observed in (Bi_{0.5}Na_{0.5})_{0.94}Ba_{0.06}TiO₃ ceramic²³ and ZnO thin films²⁰.

Figure 4 depicts temperature dependency of dielectric constant (ϵ') from 300 K to 160 K at different frequencies. At all temperatures, decreasing trend of ϵ' with the increase in frequency is observed. The decrease in ϵ' is due to polarization reduction at higher frequencies. All polarizations (electronic, ionic, interfacial etc.) react swiftly to the time-varying electric field at higher frequencies, contributing to the ϵ' . Rise in frequency of an electric field fasten the periodic reversal as much that complete dipoles cannot form in that short interval, resulting in a drop in total polarization and consequently decrease

in ϵ' ²⁵. Thermally activated dipoles assemble at grain boundaries as temperature increases that results rise in interfacial polarizations and therefore increase in ϵ' from 160 K to 300 K²⁶.

The energy losses ($\tan \delta$) of CdTiO₃ rises with the rise in temperature especially at lower frequencies as shown in Figure 5. This increase in energy loss is due to more electron exchange through resistive grain boundaries at high temperatures resulting in local electron displacement in the applied field direction²⁷. Failure of polarization mechanism at higher frequencies due to formation of incomplete dipoles is the probable cause for the drastic increase in $\tan \delta$ at higher frequencies²⁸. The low values of $\tan \delta < 1$ at all temperatures makes CdTiO₃ a potential material for electrical devices. A comparison of dielectric and electrical properties of different cadmium titanate structures is shown in Table 2.

Complex electrical modulus (M^*) is a useful tool for analyzing and visualizing electrode polarization, conductivity relaxation mechanisms and dynamical features of electrical transport mechanisms. It also emphasizes grain boundary conduction that can be difficult to distinguish from complicated impedance plots. It may also be used to distinguish between spectral

Table 2. Comparison of dielectric and electrical properties of different cadmium titanate structures

Compound	Synthesis route	Device/ Dimensions	Temperature and frequency range	Conduction mechanism (from fitting)	Minimum hopping distance (Rmin)	Density of states (DOS)	Max. Dielectric constant	Energy loss	Ref.
CdTiO ₃ Particles	Sol-gel	Disc Diameter 12mm Thickness 1 mm	623 K-873 K	-	-	-	420	2-13	29
CdTiO ₃ Particles	Solid state reaction	Disc Diameter 10 mm Thickness 1-2 mm	473 K-823 K	-	-	-	780	0.2-7.0	30
CdTiO ₃ Fibers	Electrospinning	Nanofiber	318 K-498 K	Correlated barrier hopping	0.1x10 ⁻⁹ m - 6.1x10 ⁻⁹ m	-	200	0.2-48	31
CdTiO ₃ Single Crystal	Flux grown	Glassy device Single Crystal Thickness 1.43mm, Area 4.24mm ²	298 K-923 K	Ionic hopping conduction	-	-	11000	0.5-26.5	32
CdTiO ₃ Particles (Present study)	Solid state reaction	Disc Diameter 10 mm Thickness 2 mm	160 K-300 K	Correlated barrier hopping	2.13x10 ⁻⁹ m - 1.29x10 ⁻⁷ m	0.3x10 ²¹ - 3.05x10 ²¹ eV ⁻¹ cm ⁻³	13.8	0.02-0.74	Present Study

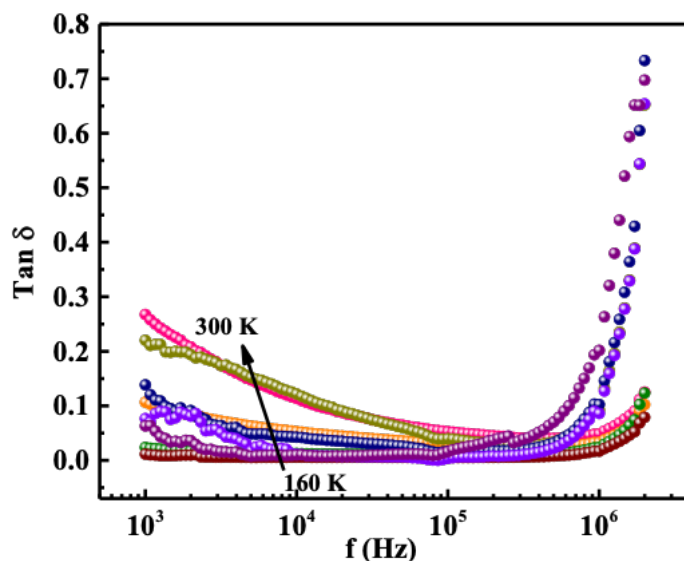


Figure 5. Frequency dependent $Tan\delta$ from 300 K to 160 K for $CdTiO_3$ nanoparticles.

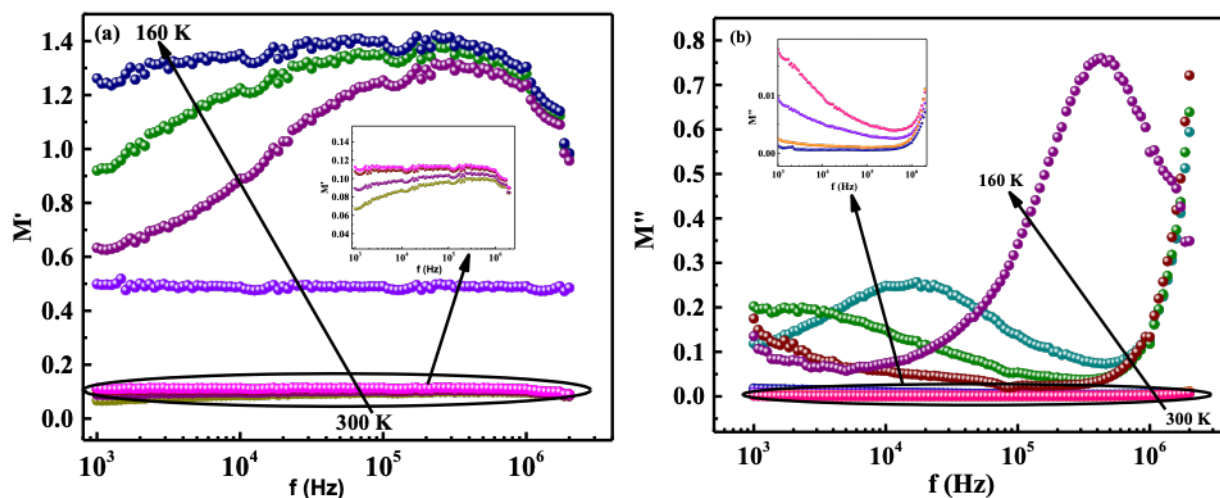


Figure 6. Frequency-dependent variation of electric modulus from 300 K to 160 K (a) real part of modulus (b) imaginary part of modulus for $CdTiO_3$ nanoparticles.

components of materials with identical resistances but varying capacitances³³. It examines the effect of grain boundary and grain on the relaxation mechanism. In the present study, the relaxation phenomena in $CdTiO_3$ have been investigated from 300 K to 160 K as a function of frequency by employing complex electric modulus³⁴. M^* comprises real (M') and imaginary (M'') parts as³⁴:

$$M^* = M' - jM'' \quad (8)$$

$$M' = \frac{\epsilon'}{\epsilon'^2 + \epsilon''^2}, M'' = \frac{\epsilon''}{\epsilon'^2 + \epsilon''^2} \quad (9)$$

where ϵ' and ϵ'' are real and imaginary parts of permittivity of $CdTiO_3$.

The M' and M'' with applied frequency are presented in Figure 6(a) and (b) from 300 K to 160 K. Figure 6(a) illustrates the frequency dependency curves of M' for $CdTiO_3$. The M' values approach towards zero at lower frequencies because of the lack of force

that governs charge carrier movement under applied electric field. This indicates the negligible electrode polarization contribution in $CdTiO_3$.³⁵ As the frequency increases, M' increases to a maximum value M'_{max} at about 0.25 MHz. Short range mobility is the possible reason of dispersion at higher frequencies³⁶. Figure 6(b) shows that M'' first decreases as frequency increases up to 0.7 MHz after that it raises to acquire maximum value from 300 K to 200 K. For temperatures less than

200 K, M'' first increases as frequency increases, get a maximum value after that it decrease and increase again. Therefore, we obtain a peak below 200 K that moves toward higher frequency side as temperature decreases. The shifting of the modulus peak is related with different relaxation time of grains and grain boundaries. As temperature decreases, the peak shifts towards higher frequencies, indicating that dielectric relaxation is a thermally triggered process where hopping is the major conduction mechanism in the material.³³ This confirms that hopping of charge carriers is the dominant conduction mechanism in CdTiO₃ as suggested from ac conductivity data.

CONCLUSIONS

CdTiO₃ nanoparticles were successfully prepared by solid-state reaction technique. XRD verify the rhombohedral structure of prepared CdTiO₃ nanoparticles. SEM image showed the presence of irregularly shaped nanoparticles. The frequency dependent electrical and dielectric properties of CdTiO₃ nanoparticles were investigated from 300 K to 160 K. The ac conductivity of CdTiO₃ follows Jonschers power law. Frequency exponent s decreased as temperature increases that showed correlate barrier hopping was dominant conduction mechanism in CdTiO₃ from 300 K to 160 K. The minimum hopping distance (R_{min}) in CdTiO₃ nanoparticles lies in the range of 2.13×10^{-9} m to 1.29×10^{-7} m. DOS for CdTiO₃ nanoparticles was calculated by the theoretical CBH model and lies in the range of $2.89 \times 10^{20} \text{ eV}^{-1}\text{cm}^{-3}$ to $2.96 \times 10^{21} \text{ eV}^{-1}\text{cm}^{-3}$. The imaginary part of the complex modulus study of CdTiO₃ nanoparticles showed the appearance of maxima at temperatures less than 200 K at different frequencies that showed different relaxation times at different temperatures.

ACKNOWLEDGMENTS

Arifa Jamil would like to acknowledge Higher Education Commission for providing IPFP fellowship under the Interim Placement of Fresh PhDs Phase-II Batch-II program at National Institute for Biotechnology and Genetic Engineering (NIBGE), Faisalabad, Pakistan. The authors declare that they have no known competing financial interests or personal relationships that could have appeared to influence the work reported in this paper.

References

- 1) Abe, H.; Kimura, Y.; Ma, T.; Tadaki, D.; Hirano-Iwata, A.; Niwano, M. Response characteristics of a highly sensitive gas sensor using a titanium oxide nanotube film decorated with platinum nanoparticles. *Sensors and Actuators B: Chemical* **2020**, *321*, 128525–128525, DOI: [10.1016/j.snb.2020.128525](https://dx.doi.org/10.1016/j.snb.2020.128525), available at <https://dx.doi.org/10.1016/j.snb.2020.128525>.
- 2) Molaei, M.; Nouri, M.; Babaei, K.; Fattah-Alhosseini, 100888; available at <https://doi.org/10.1016/j.apsadv.2021.100131>.
- 3) Jamil, S.; Fasehullah, M. Effect of Temperature on Structure, Morphology, and Optical Properties of TiO₂ Nanoparticles. *Materials Innovations* **2021**, *01* (01), 22–28, DOI: [10.54738/mi.2021.1103](https://doi.org/10.54738/mi.2021.1103), available at <https://dx.doi.org/10.54738/mi.2021.1103>.
- 4) Karunakaran, C.; Vijayabalan, A. Electrical and optical properties of polyethylene glycol-assisted sol-gel solid state reaction-synthesized nanostructured CdTiO₃. *Materials Science in Semiconductor Processing* **2013**, *16* (6), 1992–1996, DOI: [10.1016/j.mssp.2013.07.032](https://doi.org/10.1016/j.mssp.2013.07.032), available at <https://dx.doi.org/10.1016/j.mssp.2013.07.032>.
- 5) Imran, Z.; Batool, S. S.; Jamil, H.; Usman, M.; Israr-Qadir, M.; Shah, S. H.; Jamil-Rana, S.; Rafiq, M. A.; Hasan, M. M.; Willander, M. Excellent humidity sensing properties of cadmium titanate nanofibers. *Ceramics International* **2013**, *39* (1), 457–462, DOI: [10.1016/j.ceramint.2012.06.048](https://doi.org/10.1016/j.ceramint.2012.06.048), available at <https://dx.doi.org/10.1016/j.ceramint.2012.06.048>.
- 6) Mohammadi, M. R.; Fray, D. J. Low-temperature perovskite-type cadmium titanate thin films derived from a simple particulate sol-gel process. *Acta Materialia* **2009**, *57* (4), 1049–1059, DOI: [10.1016/j.actamat.2008.10.040](https://doi.org/10.1016/j.actamat.2008.10.040), available at <https://dx.doi.org/10.1016/j.actamat.2008.10.040>.
- 7) Pant, B.; Pant, H. R.; Barakat, N. A.; Park, M.; Han, T.-H.; Lim, B. H.; Kim, H.-Y. Incorporation of cadmium sulfide nanoparticles on the cadmium titanate nanofibers for enhanced organic dye degradation and hydrogen release. *Ceramics International* **2014**, *40* (1), 1553–1559, DOI: [10.1016/j.ceramint.2013.07.042](https://doi.org/10.1016/j.ceramint.2013.07.042), available at <https://dx.doi.org/10.1016/j.ceramint.2013.07.042>.
- 8) Jahanara, K.; Farhadi, S. A magnetically separable plate-like cadmium titanate-copper ferrite nanocomposite with enhanced visible-light photocatalytic degradation performance for organic contaminants. *RSC Advances* **2019**, *9* (27), 15615–15628, DOI: [10.1039/c9ra01968e](https://doi.org/10.1039/c9ra01968e), available at <https://dx.doi.org/10.1039/c9ra01968e>.
- 9) Stylianou, R.; Tkadletz, M.; Schalk, N.; Penoy, M.; Czettel, C.; Mitterer, C. Effects of reference materials on texture coefficients determined for a CVD α -Al₂O₃ coating. *Surface and Coatings Technology* **2019**, *359*, 314–322, DOI: [10.1016/j.surfcoat.2018.12.095](https://doi.org/10.1016/j.surfcoat.2018.12.095), available at <https://dx.doi.org/10.1016/j.surfcoat.2018.12.095>.
- 10) Cataño, F. A.; Gomez, H.; Dalchiele, E. A.; Marotti, R. E. Morphological and Structural Control of Electrodeposited ZnO Thin Films and Its Influence on the Photocatalytic Degradation of Methyl Orange Dye. *International Journal of Electrochemical Science* **2014**, *2014*, 534–548.
- 11) Singh, D. N.; Sinha, T. P.; Mahato, D. K. Electric modulus, scaling and ac conductivity of La₂CuMnO₆ double perovskite. *Journal of Alloys and Compounds* **2017**, *729*, 1226–1233, DOI: [10.1016/j.jallcom.2017.09.241](https://doi.org/10.1016/j.jallcom.2017.09.241), available at <https://dx.doi.org/10.1016/j.jallcom.2017.09.241>.
- 12) Batool, S. S.; Imran, Z.; Rasool, K.; Ambreen, J.; Hassan, S.; Arif, S.; Ahmad, M.; Rafiq, M. A. Study of electric conduction mechanisms in bismuth silicate nanofibers. *Scientific Reports* **2020**, *10* (1), 2775–2776, DOI: [10.1038/s41598-020-59563-6](https://doi.org/10.1038/s41598-020-59563-6), available at <https://dx.doi.org/10.1038/s41598-020-59563-6>.
- 13) Jamil, A.; Batool, S. S.; Sher, F.; Rafiq, M. A. Determination of density of states, conduction mechanisms and dielectric properties of nickel disulfide nanoparticles. *AIP Advances* **2016**, *6* (5), 055120–055120, DOI: [10.1063/1.4952966](https://doi.org/10.1063/1.4952966), available at <https://dx.doi.org/10.1063/1.4952966>.
- 14) Jonscher, A. K. Dielectric relaxation in solids. *Journal of Physics D: Applied Physics* **1999**, *32* (14), R57–R70, DOI: [10.1088/0022-3727/32/14/201](https://doi.org/10.1088/0022-3727/32/14/201), available at <https://dx.doi.org/10.1088/0022-3727/32/14/201>.
- 15) Tabib, A.; Sdiri, N.; Elhouichet, H.; Férid, M. Investigations on electrical conductivity and dielectric properties of Na doped ZnO synthesized from sol gel method. *Journal of Alloys and Compounds* **2015**, *622*, 687–694, DOI: [10.1016/j.jallcom.2014.10.092](https://doi.org/10.1016/j.jallcom.2014.10.092).

- available at <https://dx.doi.org/10.1016/j.jallcom.2014.10.092>.
- 16) Ganaie, M.; Zulfueqar, M. AC Conductivity Measurement of Cd₅Se₉–xZn_x Chalcogenide Semiconductor Using Correlated Barrier Hopping Model. 2015; available at <https://dx.doi.org/10.12693/aphyspola.128.59>.
- 17) Ghosh, A. ac conduction in iron bismuthate glassy semiconductors. *Physical Review B* **1990**, *42* (2), 1388–1393.
- 18) Meaz, T. M.; Attia, S. M.; Ata, A. M. A. E. Effect of tetravalent titanium ions substitution on the dielectric properties of Co–Zn ferrites. *Journal of Magnetism and Magnetic Materials* **2003**, *257* (2-3), 296–305, DOI: [10.1016/s0304-8853\(02\)01212-x](https://doi.org/10.1016/s0304-8853(02)01212-x), available at [https://dx.doi.org/10.1016/s0304-8853\(02\)01212-x](https://dx.doi.org/10.1016/s0304-8853(02)01212-x).
- 19) Austin, I. G.; Mott, N. F. Polarons in crystalline and non-crystalline materials. *Advances in Physics* **1969**, *18* (71), 41–102, DOI: [10.1080/00018736900101267](https://doi.org/10.1080/00018736900101267), available at <https://dx.doi.org/10.1080/00018736900101267>.
- 20) Jamil, A.; Fareed, S.; Tiwari, N.; Li, C.; Cheng, B.; Xu, X.; Rafiq, M. A. Effect of titanium doping on conductivity, density of states and conduction mechanism in ZnO thin film. *Applied Physics A* **2019**, *125* (4), DOI: [10.1007/s00339-019-2544-6](https://doi.org/10.1007/s00339-019-2544-6), available at <https://dx.doi.org/10.1007/s00339-019-2544-6>.
- 21) Ojha, S.; Ali, M. S.; Roy, M.; Bhattacharya, S. Hopping frequency and conductivity relaxation of promising chalcogenides: AC conductivity and dielectric relaxation approaches. *Materials Research Express* **2021**, *8* (8), 085203–085203, DOI: [10.1088/2053-1591/ac1d17](https://doi.org/10.1088/2053-1591/ac1d17), available at <https://dx.doi.org/10.1088/2053-1591/ac1d17>.
- 22) Lily, Kumari, K.; Prasad, K.; Choudhary, R. N. P. Impedance spectroscopy of (Na_{0.5}Bi_{0.5})(Zr_{0.25}Ti_{0.75})O₃ lead-free ceramic. *Journal of Alloys and Compounds* **2008**, *453* (1-2), 325–331, DOI: [10.1016/j.jallcom.2006.11.081](https://doi.org/10.1016/j.jallcom.2006.11.081), available at <https://dx.doi.org/10.1016/j.jallcom.2006.11.081>.
- 23) Roy, A. K.; Singh, A.; Kumari, K.; Nath, K. A.; Prasad, A.; Prasad, K. Electrical Properties and AC Conductivity of (Bi_{0.5}Na_{0.5})_{0.94}Ba_{0.06}TiO₃ Ceramic. *ISRN Ceramics* **2012**, 1–10.
- 24) Prasad, K.; Lily, Kumari, K.; Chandra, K. P.; Yadav, K. L.; Sen, S. Electrical properties of a lead-free perovskite ceramic: (Na_{0.5}Sb_{0.5})TiO₃. *Applied Physics A* **2007**, *88* (2), 377–383, DOI: [10.1007/s00339-007-3989-6](https://doi.org/10.1007/s00339-007-3989-6), available at <https://dx.doi.org/10.1007/s00339-007-3989-6>.
- 25) Charoonsuk, T.; Sriphan, S.; Pulphol, P.; Vittayakorn, W.; Vittayakorn, N.; Maluangnont, T. AC Conductivity and Dielectric Properties of Lepidocrocite-type Alkali Titanate Tunable by Interlayer Cation and Intralayer Metal. *Inorganic Chemistry* **2020**, *59* (21), 15813–15823, DOI: [10.1021/acs.inorgchem.0c02264](https://doi.org/10.1021/acs.inorgchem.0c02264), available at <https://dx.doi.org/10.1021/acs.inorgchem.0c02264>.
- 26) Rathan, S. V.; Govindaraj, G. Thermal and electrical relaxation studies in Li(4+x)TixNb1–xP3O12 (0.0 ≤ x ≤ 1.0) phosphate glasses. *Solid State Sciences* **2010**, *12* (5), 730–735, DOI: [10.1016/j.solidstatesciences.2010.02.030](https://doi.org/10.1016/j.solidstatesciences.2010.02.030), available at <https://dx.doi.org/10.1016/j.solidstatesciences.2010.02.030>.
- 27) Mir, S. A.; Ikram, M.; Sultan, K.; Habib, Z.; Kausar, H.; Asokan, K. Correlative Exploration Of Structural, Optical And Electric Properties Of Colossal Dielectric Ni Doped Sm Orthoferrites. *Advanced Materials Letters* **2015**, *6* (12), 1081–1087, DOI: [10.5185/amlett.2015.5959](https://doi.org/10.5185/amlett.2015.5959), available at <https://dx.doi.org/10.5185/amlett.2015.5959>.
- 28) Dong, G.; Tan, G.; Luo, Y.; Liu, W.; Ren, H.; Xia, A. Investigation of Tb-doping on structural transition and multiferroic properties of BiFeO₃ thin films. *Ceramics International* **2014**, *40* (5), 6413–6419, DOI: [10.1016/j.ceramint.2013.11.089](https://doi.org/10.1016/j.ceramint.2013.11.089), available at <https://dx.doi.org/10.1016/j.ceramint.2013.11.089>.
- 29) Bahloul, R.; Sayouri, S.; Lamcharfi, T. Dielectric and ac conductivity of ilmenite-type CdTiO₃ ceramic. *Mediterranean Journal of Chemistry* **2019**, *8* (3), 255–260, DOI: [10.13171/mjc8319052407rb](https://doi.org/10.13171/mjc8319052407rb), available at <https://dx.doi.org/10.13171/mjc8319052407rb>.
- 30) Acharya, T.; Choudhary, R. N. P. Development of ilmenite-type electronic material CdTiO₃ for devices. *IEEE Transactions on Dielectrics and Electrical Insulation* **2015**, *22* (6), 3521–3528, DOI: [10.1109/tdei.2015.005196](https://doi.org/10.1109/tdei.2015.005196), available at <https://dx.doi.org/10.1109/tdei.2015.005196>.
- 31) Imran, Z.; Rafiq, M. A.; Ahmad, M.; Rasool, K.; Batool, S. S.; Hasan, M. M. Temperature dependent transport and dielectric properties of cadmium titanate nanofiber mats. *AIP Advances* **2013**, *3* (3), 032146–032146, DOI: [10.1063/1.4799756](https://doi.org/10.1063/1.4799756), available at <https://dx.doi.org/10.1063/1.4799756>.
- 32) Gupta, V.; Bamzai, K. K.; Kotru, P. N.; Wanklyn, B. M. Dielectric properties, ac conductivity and thermal behaviour of flux grown cadmium titanate crystals. *Materials Science and Engineering: B* **2006**, *130* (1-3), 163–172, DOI: [10.1016/j.mseb.2006.03.006](https://doi.org/10.1016/j.mseb.2006.03.006), available at <https://dx.doi.org/10.1016/j.mseb.2006.03.006>.
- 33) Oruç, P.; Turan, N.; Demirölmez, Y.; Seçkin, A.; Çavdar, Ş.; Koralay, H.; Tuğluoğlu, N. AC conductivity, dielectric and electrical modulus studies of bulk Zn_{0.95}Co_{0.05}O ceramic. *Journal of Materials Science: Materials in Electronics* **2021**, *32* (12), 15837–15850, DOI: [10.1007/s10854-021-06136-6](https://doi.org/10.1007/s10854-021-06136-6), available at <https://dx.doi.org/10.1007/s10854-021-06136-6>.
- 34) Nasri, M.; Henchiri, C.; Dhahri, R.; Khefifi, J.; Rahmouni, H.; Dhahri, E.; Omari, L. H.; Tozri, A.; Berber, M. R. Structural, dielectric, electrical and modulus spectroscopic characteristics of CoFeCuO₄ spinel ferrite nanoparticles. *Materials Science and Engineering: B* **2021**, *272*, 115331–115331, DOI: [10.1016/j.mseb.2021.115331](https://doi.org/10.1016/j.mseb.2021.115331), available at <https://dx.doi.org/10.1016/j.mseb.2021.115331>.
- 35) Chatterjee, B.; Gupta, P. N. Nanocomposite films dispersed with silica nanoparticles extracted from earthworm humus. *Journal of Non-Crystalline Solids* **2012**, *358* (23), 3355–3364, DOI: [10.1016/j.jnoncrysol.2012.08.020](https://doi.org/10.1016/j.jnoncrysol.2012.08.020), available at <https://dx.doi.org/10.1016/j.jnoncrysol.2012.08.020>.
- 36) Chérif, S. F.; Chérif, A.; Dridi, W.; Zid, M. F. Ac conductivity, electric modulus analysis, dielectric behavior and Bond Valence Sum analysis of Na₃Nb₄As₃O₁₉ compound. *Arabian Journal of Chemistry* **2020**, *13* (6), 5627–5638, DOI: [10.1016/j.arabjc.2020.04.003](https://doi.org/10.1016/j.arabjc.2020.04.003), available at <https://dx.doi.org/10.1016/j.arabjc.2020.04.003>.